Journal of Materials Science & Technology 158 (2023) 218–225

Contents lists available at ScienceDirect

Journal of Materials Science & Technology

journal homepage: www.elsevier.com/locate/jmst

Research Article

Nanoscale fluctuation of stacking fault energy strengthens multi-principal element alloys

Zongrui Pei[a,b,*], Markus Eisenbach[b], Peter K. Liaw[c], Mingwei Chen[d,e]

[a] New York University, New York 10012, USA
[b] Oak Ridge National Laboratory, Oak Ridge, Tennessee 37831, USA
[c] Department of Materials Science and Engineering, The University of Tennessee, Knoxville, TN 37996, USA
[d] Department of Materials Science and Engineering, Johns Hopkins University, Baltimore, Maryland 21218, USA
[e] Engineering and Hopkins Extreme Materials Institute, Johns Hopkins University, Baltimore, Maryland 21218, USA

ARTICLE INFO

Article history:
Received 25 November 2022
Revised 7 January 2023
Accepted 12 January 2023
Available online 29 March 2023

Keywords:
Nanoscale energy fluctuation
Staking fault energy
Chemical short-range order
Multi-principal element alloy
Mechanism

ABSTRACT

Chemical randomness and the associated energy fluctuation are essential features of multi-principal element alloys (MPEAs). Due to these features, nanoscale stacking fault energy (SFE) fluctuation is a natural and independent contribution to strengthening MPEAs. However, existing models for conventional alloys (i.e., alloys with one principal element) cannot be applied to MPEAs. The extreme values of SFEs required by such models are unknown for MPEAs, which need to calculate the nanoscale volume relevant to the SFE fluctuation. In the present work, we developed an analytic model to evaluate the strengthening effect through the SFE fluctuation, profuse in MPEAs. The model has no adjustable parameters, and all parameters can be determined from experiments and *ab initio* calculations. This model explains available experimental observations and provides insightful guidance for designing new MPEAs based on the SFE fluctuation. It generally applies to MPEAs in random states and with chemical short-range order.

1. Introduction

Energy fluctuations due to chemical randomness are profuse in multi-principal element alloys (MPEAs), one group of extensively studied alloys [1–9]. The observations of chemical short-range order (CSRO) in MPEAs render their chemical disorder an interesting topic [10–12]. Hitherto there is a lack of analytic models to quantitatively evaluate the various contributions to the mechanical properties, such as the strengthening effect due to the stacking fault energy (SFE) fluctuation in MPEAs.

The strengthening effect through SFE (γ_{SFE}) has been investigated for decades in conventional face-centered-cubic (fcc) alloys (i.e., alloys with one principal element) [13,14]. Driven by thermodynamics, solutes usually segregate at cores of partial dislocations and the stacking faults (SFs). When dislocations move, they have to escape from the trapping of these solutes, which increases the energy cost to move dislocations and thus strengthens the alloys. The solute-dislocation interaction is a key quantity in almost all classic dislocation models. It consists of elastic and chemical interactions between solutes and SFs. The chemical interaction is described by a parameter $\epsilon_{SFE} = \mathrm{d}\ln(\gamma_{SFE})/\mathrm{d}c_s|_{c_s=0}$ (c_s is the solute concentration) [14,15]. This effect is attributed to the change of SFE upon alloying, common in conventional alloys. In MPEAs, the roles of solutes and solvents are not well defined for constituting atoms, which makes it difficult to define ϵ_{SFE} for MPEAs. Nonetheless, the strengthening effect introduced by the change of the *averaged* SFE can still be considered using density functional theory (DFT), and multiscale models [16]. At the same time, another independent contribution to the yield stresses becomes more significant, i.e., the strengthening through the nanoscale SFE fluctuation. This feature is signified by the varying distances between two Shockley partials and the curved dislocation lines [see Fig. 1 (a, b)]. Although some studies have shown SFE fluctuations play a role in strengthening alloys [17,18], there is a lack of full models to quantify the strengthening effect in MPEAs analytically.

The nanoscale SFE fluctuation finds its origin in the diverse interatomic interactions. The multiple origins that lead to these fluctuations, e.g., CSRO and lattice distortion, have been widely acknowledged [5,10,19–21]. The CSRO effect on mechanical properties recently has become one of the main foci in high-entropy solid solutions (Fig. 1 (c)) [10,12,22–30]. This contribution may not be essential for conventional alloys. The SFE fluctuation in such alloys is usually weaker than in MPEAs, due to their less complex bonding characters and fewer allowable configurations. Thus, in con-

* Corresponding author.
E-mail addresses: peizongrui@gmail.com, zp2137@nyu.edu (Z. Pei).

https://doi.org/10.1016/j.jmst.2023.01.042
1005-0302/

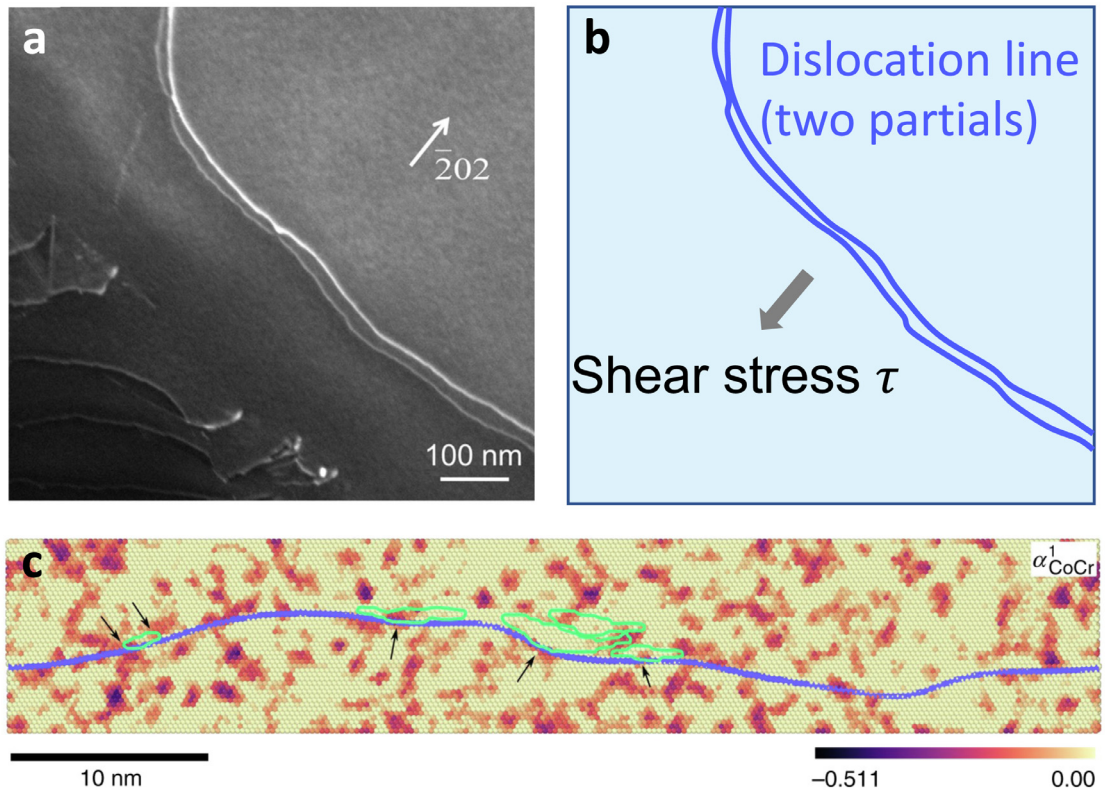

Fig. 1. Dislocations in multi-principal element alloys. (a) A dissociated dislocation with both Shockley partials visible under weak beam dark field scanning transmission electron microscopy (WB DF STEM) in NiCoCr [24]; (b) The curved dislocation line is extracted from the STEM image for better visualization; (c) A curved dislocation in NiCoCr with CSRO by molecular dynamics at 300K [8]. The CSRO of the nearest-neighbor Co-Cr pair α_{CoCr} is adopted to color the atoms. The green lines circle the slipped areas.

ventional alloys, one of the main contributions to yielding is the strengthening effect through the SFE difference caused by precipitation [17,31,32].

It is not straightforward to determine the extreme values of the SFE fluctuation in precipitate-free solid solutions. We will demonstrate that the classic strengthening models are still useful, with appropriate adjustments, once we can find the SFE distribution as a function of the alloy system, temperature (it affects CSRO), etc. Our theoretical framework consists of several models, including two recently developed theories. The first theory is Pei's statistical method to evaluate the fluctuation of SFEs [21], which is based on the third law of thermodynamics; the second one is the Varvenne model that provides a pathway to calculate the relevant volume for the SFE fluctuation [33]. It is worth mentioning the Varvenne model is adopted only as a technique to calculate the volume and the model framework is not used here and different from this study. In this framework, the physically relevant volume is determined by a box whose three dimensions are at the nanoscale. The fluctuation of SFE is naturally determined without any adjustable parameters. The model is able to calculate the magnitude of the strengthening effect through nanoscale energy fluctuations, and it can help to understand the underlying physical mechanisms in experimental observations and provide guidance for alloy design.

2. Computational details

Spin-polarized and non-spin-polarized density functional theory (DFT) [34,35] simulations are carried out using Vienna *Ab-initio* Simulation Package (VASP) [36] to obtain the total energies for the stacking fault energy (SFE) calculations. The generalized gradient approximation (GGA) parametrized by Perdew-Burke-Ernzerhof (PBE) [37] is used to calculate the electronic exchange-correlation interaction, and the Kohn-Sham equation is solved employing the projector augmented wave (PAW) method [38], where the Brillouin zone is sampled using Monkhorst-Pack scheme [39]. The atomic configurations of elements in the pseudo potentials used in our calculations are Co $[Ar]3d^84s^1$, Cr $[Ar]3d^54s^1$, Ni $[Ar]3d^84s^2$, Mn $[Ar]3d^64s^1$, Fe$[Ar]3d^74s^1$, and V $[Ne3s^2]3p^63d^34s^2$. Supercells of 72 atoms are employed to calculate SFEs for Ni, VCoNi, NiCoCr, and CoCrFeNiMn. The stacking fault is introduced by shifting the upper half supercell along the Burgers vector of the Shockley partial dislocation relative to the lower half. Once the lattice constants are optimized, only the ionic positions are relaxed in the SFE calculations, the supercell shape and volume are fixed (ISIF=2). This is sufficient since we are interested in the trend of SFE changes. The relaxation stops when the energy difference between ionic steps is smaller than 10^{-4} eV. A plane wave cutoff of 350 eV and the k-point meshes of $6 \times 4 \times 4$ for Brillouin zone are used. An increase of *k*-point meshes by 8 times ($2 \times 2 \times 2$), the change in total energy is less than 2 meV or 0.028 meV/atom.

The elastic constants and Burgers vectors for NiCoCr and CoCrFeNiMn are adopted from Ref. [33]. We obtained these parameters for VCoNi from our DFT calculations based on a single-crystal supercell of 72 atoms, i.e., $G = 77.7$ GPa, $b = 2.53$ Å; Poisson ratio ν is taken as 0.33, which is an average of the experimental values of the pure elements. These numbers are in good agreement with the experimentally measured values [40], i.e., $G = 72$ GPa, $b = 2.55$ Å, and Poisson ratio $\nu = 0.33$.

3. Model development and results

3.1. Strengthening model for the SFE fluctuation in MPEAs

The development of our model starts with the classic model for alloy strengthening through the variance of *averaged* SFE. The model was frequently mentioned in the literature, such as the

seminal paper of Hirsch and Kelly [31]. It applies to the presence of precipitates, by assuming the SFEs of precipitates and the matrix are different. Here the SFEs of the matrix and the precipitate particles are well defined. This is essentially different from MPEAs, which is a single-phase solid solution. The SFE fluctuates and varies locally, but the magnitude of this fluctuation is unknown. Here we will generalize this approach to treat the effect generated by the latter.

For a general stress state $\boldsymbol{\sigma}$, the force on a dislocation $\boldsymbol{b}$ is given by the Peach-Koehler equation of $\boldsymbol{F} = (\boldsymbol{\sigma} \cdot \boldsymbol{b}) \times \boldsymbol{s}$ with $\boldsymbol{b}$ and $\boldsymbol{s}$ as the Burgers vector and unit vector of the line direction. There are force equilibrium equations both for the trailing and leading partial dislocations. When SFE is positive, we have

$$-\frac{K}{d_{12}} + \gamma_1 + (\boldsymbol{\sigma} \cdot \boldsymbol{b}_1) \times \boldsymbol{s} = 0, \tag{1a}$$

$$\frac{K}{d_{12}} - \gamma_2 + (\boldsymbol{\sigma} \cdot \boldsymbol{b}_2) \times \boldsymbol{s} = 0. \tag{1b}$$

Here the constant K is a combination of elastic constants and Burgers vector, i.e., $K = \frac{\mu b^2}{24\pi}\frac{2+\nu}{1-\nu}$, where μ, ν are the shear modulus and Poisson ratio, respectively. γ_1, γ_2 are the SFEs experienced by partials $\boldsymbol{b}_1$, $\boldsymbol{b}_2$. Since the random solutes are not uniformly distributed, the associated energy fluctuation results in different SFEs locally. The strengthening due to the SFE fluctuation is

$$\tau_\gamma = \frac{[\boldsymbol{\sigma} \cdot (\boldsymbol{b}_1 + \boldsymbol{b}_2)] \times \boldsymbol{s}}{b} = \frac{\gamma_2 - \gamma_1}{b}. \tag{2}$$

Calculating the difference $\Delta\gamma = \gamma_1 - \gamma_2$ is a statistical problem, which requires knowledge about the distribution of SFE γ around its average $\bar{\gamma} = \gamma_0$.

It is not difficult to measure SFE γ_0 in experiment or calculate it theoretically. For NiCoCr and some other MPEAs, γ_0 =20–30 mJ m^{-2} [20,41,42]. However, we know very little about its distribution, although its existence can be deduced indirectly from molecular dynamics [8,33,43]. Thus, we assume a distribution for γ, and in view of the limited knowledge, a Gaussian distribution $N(\gamma; \bar{\gamma}, \sigma_\gamma^2)$ is a natural choice with σ_γ^2 as the variance [see Fig. 2]. In the presence of precipitates and clustered ordering [10], the strengthening is determined by the maximum $\Delta\gamma$, i.e.,

$$\tau_\gamma = \frac{(\bar{\gamma} + \sigma_\gamma) - (\bar{\gamma} - \sigma_\gamma)}{b} = \frac{2\sigma_\gamma}{b}. \tag{3}$$

In homogeneous solid solutions without clustered ordering, the averaged τ is more relevant, $\tau_\gamma = \overline{\tau} = \frac{1}{L}\int \tau(l)dl$ [see Fig. 2(c) for the parameter definitions and the schematic]. We need to determine the distribution of $\Delta\gamma$ to find $\bar{\tau}$.

Assuming $N(\gamma; \bar{\gamma}, \sigma_\gamma^2)$ is known, one can easily find the distribution for $\Delta\gamma$, i.e., $\Delta\gamma \sim N(\Delta\gamma; \bar{\gamma} - \bar{\gamma}, \sigma_\gamma^2 + \sigma_\gamma^2) = N(\Delta\gamma; 0, 2\sigma_\gamma^2)$. Since there is a strengthening effect only when $\Delta\gamma = \gamma_1 - \gamma_2 > 0$, the SFE fluctuation actually follows a half-Gaussian distribution $f(\Delta\gamma)$, i.e., $f(\Delta\gamma) = N(\Delta\gamma; 0, 2\sigma_\gamma^2)$, $\Delta\gamma > 0$; $f(\Delta\gamma) = 0, \Delta\gamma \le 0$. The expectation of $\Delta\gamma$ is $\overline{\Delta\gamma} = 2\int_0^{+\infty} N(\Delta\gamma; 0, 2\sigma_\gamma^2)\Delta\gamma d\Delta\gamma = \frac{2}{\sqrt{\pi}}\sigma_\gamma$ and standard variance $\sigma_\gamma'^2 = 2(1-2/\pi)\sigma_\gamma^2$. The average $\Delta\gamma$ fluctuates mainly within a range of $[\frac{2}{\sqrt{\pi}}\sigma_\gamma - \sigma_\gamma', \frac{2}{\sqrt{\pi}}\sigma_\gamma + \sigma_\gamma']$. The relations between these parameters are summarized in Table 1. Then we have the following equation to calculate the strengthening effect,

$$\tau_\gamma = \frac{\gamma_1 - \gamma_2}{b} = \frac{1}{\sqrt{\pi}}\frac{2\sigma_\gamma}{b}. \tag{4}$$

The above two cases can be combined as

$$\tau_\gamma = C_0\frac{2\sigma_\gamma}{b}, \tag{5}$$

where $C_0 = 1/\sqrt{\pi} \approx 0.564$ for random solid solutions and $C_0 = 1$ when clustered ordering is present. When CSRO forms, a fraction of the total energy states is preferred over the others, for which the Gaussian distribution can still hold approximately. Strong ordering (e.g., the formation of intermetallics) will even split it into two separate Gaussian distributions with average SFEs γ_1 and γ_2. As a consequence, σ_γ becomes larger, and the strengthening effect becomes stronger. Areas with strong CSRO are similar to precipitates, where the clustered-ordering model applies ($C_0 = 1$). Compared to the model for random solid solutions ($C_0 = 1/\sqrt{\pi}$), the stronger strengthening effect can be attributed to CSRO. Therefore, the strengthening effect of CSRO is reflected by both the constant C_0 and the standard variance σ_γ.

While it is not straightforward to measure or calculate the fluctuation of γ, we will find the physically relevant value for σ_γ.

Table 1
Parameters for the distributions. The relations between these parameters provide a pathway to accurately calculate them by DFT.

Quantity	Distribution	Expectation	Variance
γ	Gaussian	$\bar{\gamma}$ (γ_0)	σ_γ^2
$\gamma_1 - \gamma_2$	Gaussian	0	$2\sigma_\gamma^2$
$\gamma_1 - \gamma_2 \ge 0$	half-Gaussian	$2\sigma_\gamma/\sqrt{\pi}$	$2(1-2/\pi)\sigma_\gamma^2$

3.2. Energy fluctuation in MPEAs

We adopt and adjust a statistical theory developed by us to approximate σ_γ in the random state, which is needed to further determine the strengthening effect of SFE fluctuations [21]. The theory was originally developed to evaluate the magnitude of thermodynamic fluctuation and is adopted here to construct a strengthening model. Generally, the standard deviation of energies for a system is given by

$$\epsilon_E = \sqrt{\frac{1}{N_\mathrm{m} - 1}\sum_i (E_i - \langle E_i\rangle)^2} = \sqrt{\langle E_i^2\rangle - \langle E_i\rangle^2}, \tag{6}$$

where E_i is the energy of configuration i out of the total N_m configurations. When N_m is sufficiently large, the error bar is independent of N_m and becomes a constant that is not necessarily zero. Assuming the number of configurations as a function of energy, i.e., the configurational density of states (DOS), follows a Gaussian distribution $N(E; \mu_E, \sigma_E)$, we find

$$\lim_{N_\mathrm{m}\to+\infty} \epsilon_E = \sigma_E \neq 0. \tag{7}$$

Here σ_E is the standard variance of the entirety and μ_E is the average energy $\langle E\rangle$. If the sample space is very limited (i.e., a small system and large σ_E), the energies have a large standard variance that cannot be smaller than σ_E.

It has been confirmed that the DOS $g(E)$ indeed follows a Gaussian distribution, such as in the theoretic studies of NiCoCr [21,44], FeCo [21,45] and CuZn [46]. When $g(E) = N(E; \mu_E, \sigma_E) = 1/\sqrt{2\pi(\sigma_E/\Delta E)^2}\exp(-\frac{(E-\mu_E)^2}{2\sigma_E^2})$, $\ln[g(E)]$ must be a parabolic function such as $\ln[g(E)] = a(E - E_\mathrm{random})^2 + b$ ($a < 0, b > 0$) with $E_\mathrm{random} = \mu_E$, $a = -1/2\sigma^2$, $b = -1/2\ln(2\pi\sigma^2) + C_0$ and $C_0 = \ln(\Omega)$. Here Ω is the total number of configurations with system size N_s and $\Delta E = E_\mathrm{min} - E_\mathrm{random}$. The $\ln(g(E))$ of CuZn [46], FeCo and NiCoCr [45] obtained using Wang-Landau Monte Carlo method indeed have parabolic shapes. The exact $\ln[g(E)]$ for finite systems may be slightly affected by crystal structure, constitution (chemical species, and the number of them N_c, and concentrations $\{c_i\}$), system's geometric shape and size N_s.

According to the third law of thermodynamics, the lowest energy E_min corresponds to a unique and ordered state (when spatially degenerate states are considered as one state), resulting in $\ln(g(E_\mathrm{min})) = 0$. For an equiatomic N_c-component sys-

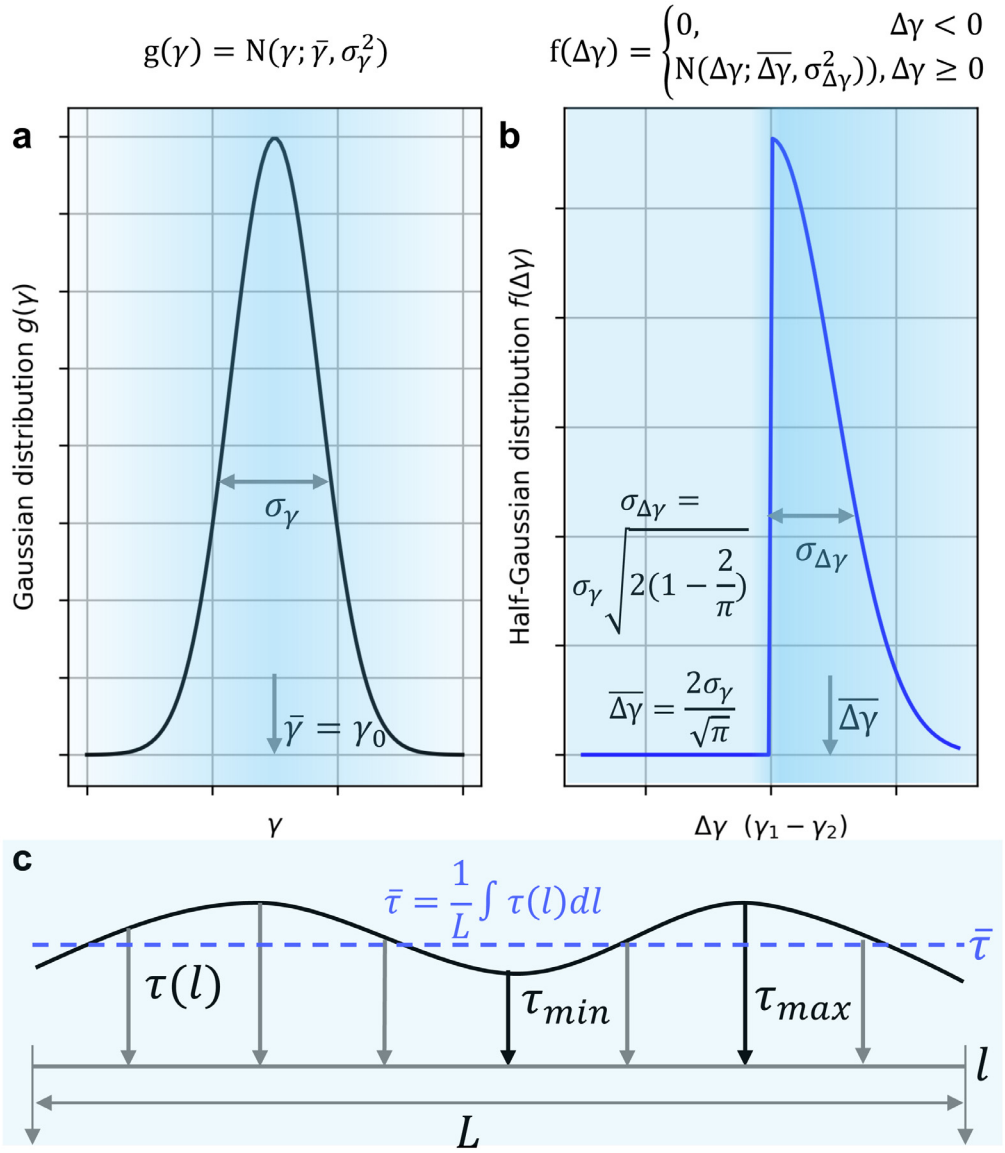

Fig. 2. Gaussian distribution for SFE and its corresponding half distribution. Since both γ_1 and γ_2 follow the same Gaussian distribution $g(\gamma)$ (a), their difference $\Delta\gamma$ is also a Gaussian distribution albeit with a zero average and a different variance $2\sigma_\gamma^2$. The physically meaningful distribution $f(\Delta\gamma)$ is a half-Gaussian distribution (b), because a negative difference does not have the strengthening effect. (c) Schematic for evaluating the strengthening through SFE fluctuation.

tem, this equation is equivalent to $N_s = \frac{(\Delta E)^2}{2\sigma_E^2 \ln(N_c)} + \frac{\ln(2\pi(\sigma_E/\Delta E)^2)}{2\ln(N_c)} \approx \frac{(\Delta E)^2}{2\sigma_E^2 \ln(N_c)}$. For a non-equiatomic system of concentrations $\{c_i\}$, the equation can be written as

$$\sigma_E = \frac{\Delta E}{\sqrt{2N_s f(\{c_i\})}}, \tag{8}$$

where $f(\{c_i\}) = -\sum_i c_i \ln(c_i)$. This equation is derived by Pei and validated by the accurate Wang-Landau MC method [21]. Assuming that the lattice parameters of the random and ordered states are the same, we have similar relation for the fluctuation of SFE σ_γ. Thus, the energy fluctuation σ_E is related to σ_γ by a constant, i.e., the SF area A, which yields the SFE fluctuation $\sigma_\gamma = \sigma_E/A$. The assumption that SFE follows a Gaussian distribution is directly confirmed elsewhere using an empirical potential [47].

For one specific system, A, $f(\{c_i\})$ and ΔE are the same. Hence, the standard deviations of different system sizes N_{s1}, N_{s2} have a simple relationship $\sigma_{\gamma 2} = \sigma_{\gamma 1}\sqrt{N_{s1}/N_{s2}}$. This provides a useful method to calculate the SFE fluctuation from DFT,

$$\sigma_\gamma = \sigma_{\gamma,\mathrm{DFT}}\sqrt{\frac{N_{\mathrm{DFT}}}{N_s}}. \tag{9}$$

Eq. (9) is a special case of Eq. (8). Both Eq. (8) and Eq. (9) can be used to evaluate σ_γ, depending on the physical quantities that are readily available for calculations. Note that we need to randomly sample the system and not use special quasirandom structures(SQS) [48]. The SQS method picks the most random structures, which makes the sampling biased and $\sigma_{\gamma,\mathrm{DFT}}$ smaller than its actual value. The averaged SFE and the SFE fluctuation $\sigma_{\gamma,\mathrm{DFT}}$ are calculated and plotted in Fig. 3 for the example of NiCoCr. Multiple random configurations for the calculations of one SFE, which allows us to evaluate the average and variance of the SFE. The averaged SFEs for NiCoCr become converged with a sufficiently large number of calculations. One key message we utilize to develop our method is that the standard variance depends on system size. Theoretically, any sufficiently large system can be used to calculate the standard variance [21], assisted by Eq. 9. When $\sigma_{\gamma,\mathrm{DFT}}$ is converged,

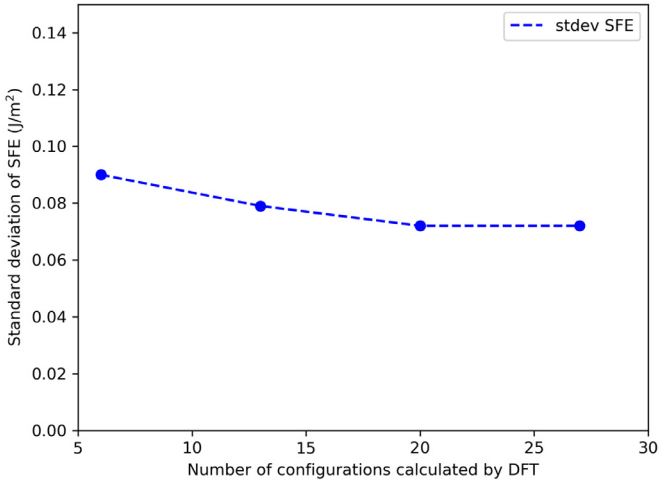

Fig. 3. Dependence of the standard variance of SFEs on the number of calculations/configurations (NiCoCr). The standard deviation converges as the number of calculations increases. The converged standard deviation is not an error bar but a property that reflects the supercell size used in the calculations.

our model prediction will not be affected, which is confirmed in Fig. 3 for the case of NiCoCr.

We can calculate a particular σ from DFT but we do not know the system size N (i.e., $N_{s,2}$ in the above equation) that is relevant to the actual SFE fluctuation. We need to determine a physically relevant N_s or its volume size for the strengthening effect.

Volume size relevant to SFE fluctuation— One natural method to determine N_s is through a volume V_a defined in Fig. 4, which is basically the volume around one typical kink. Once we know the volume, we can calculate the number of atoms that it includes by

$$N_s = 2N_{(111)} \times \frac{\xi_c}{\sqrt{3}b} \times \frac{d_{12}}{b}, \tag{10}$$

where $N_{(111)}$ is the number of (111) planes in which solutes contribute significantly to the dislocation-solute interaction. The factor 2 comes from the number of atoms in the area $\sqrt{3}b \times b$. d_{12} is the SF width, and ξ_c is the length of the straight dislocation segment, which is equivalent to the critical length in Varvenne model determined by the variational principle [33].

From the classic dislocation theory, we know that the interaction between solute and dislocation is nearsighted [49–52]. This has been demonstrated by the predictive solute-solution strengthening model of Ma et al. [49] and the convergence test of Leyson et al. [50] Nonetheless it will be shown later that the number of layers perpendicular to the SF plane is not important, and we only need to keep the chosen layers the same as the sampled layers in DFT. The key parameter is the SF area that determines the number of atoms along the other two directions. The second term that we need to know in the equation of V_a is the SF width between Shockley partials, which can be approximated by $d_{12} = \frac{Gb}{\gamma_0}\frac{b}{24\pi}\frac{2+\nu}{1-\nu}$. Here γ_0 is the SFE at finite temperatures that can be determined both from DFT calculations or experimentally.

The Varvenne model provides a variational method to approximate ξ_c (or N) [33]. The basic idea of the model is to find a balance between (i) the line tension Γ of a dislocation that tends to shorten its length and (ii) the solute-dislocation interaction that tends to increase it. This results in a zigzag dislocation [see Fig. 4(a)]. The key quantity is the relative total energy for a dislocation

$$\Delta E_{\text{tot}}(\xi, w) = \left[\Gamma\frac{w^2}{2\xi} - \left(\frac{\xi}{\sqrt{3}b}\right)^{\frac{1}{2}}\Delta\tilde{E}_p(w)\right]\left(\frac{L}{2\xi}\right), \tag{11}$$

where $\Delta\tilde{E}_p(w)$ is the energy associated with the solute-dislocation interaction, which is a function of the glide distance w. Minimizing $\Delta E_{\text{tot}}(\xi, w)$ gives the critical length $\xi_c(w_c)$

$$\xi_c(w_c(d_{12})) = \left(4\sqrt{3}\frac{\Gamma^2 w_c^4 b}{\Delta\tilde{E}_p^2(w_c)}\right)^{\frac{1}{3}}. \tag{12}$$

The involved parameters are illustrated in Fig. 4. It is worth mentioning that this analytical technique is just one of the possible methods to calculate ξ_c that appeared in Eq. (10). We can choose a different method to evaluate the parameter. To avoid potential confusion, we also want to point out that our model is not based on the model of Varvenne et al.. Instead, the theoretical framework of this work is based on the seminal paper of Hirsch and Kelly [31]. We follow the procedure described in Varvenne et al. [33] to obtain ξ_c. More technical details are referred to in this literature.

We use NiCoCr as an example to show the calculation of ξ_c. After minimizing the total energy ΔE_{tot} [see Fig. 5(a)], we can determine the critical dislocation glide width w_c and length ξ_c (Fig. 5(b)). For NiCoCr, we find ξ_c is about 20–35 units of $\sqrt{3}b$, which is overall approximately 25 $\times\sqrt{3}b$. At a large SF width (or low SFE), the critical length converges to 29 $\times\sqrt{3}b$. Similar critical lengths are obtained for VCoNi ($26 \times \sqrt{3}b$) and the Cantor alloy ($31 \times \sqrt{3}b$) (see the supplementary material).

3.3. Full model and reduced model

The full model consists of a series of coupled equations through the SFE γ. A simplified version of these equations is

$$\tau_\gamma = \frac{2C_0\sigma_\gamma}{b}; \tag{13a}$$

$$\sigma_\gamma = \sigma_{\gamma,\text{DFT}}\sqrt{\frac{N_{\text{DFT}}}{N_s}} \text{ or } \sigma_\gamma = \frac{\Delta E}{A\sqrt{2N_s f(\{c_i\})}}; \tag{13b}$$

$$N_s = 2N_{(111)}\frac{\xi_c}{\sqrt{3}b}\frac{d_{12}}{b}; \tag{13c}$$

$$\xi_c = \xi_c(d_{12}); \tag{13d}$$

$$d_{12}(\gamma) \approx \frac{Gb}{\gamma}\frac{b}{24\pi}\frac{2+\nu}{1-\nu}. \tag{13e}$$

As stated above, these equations correspond to (i) the newly developed strengthening theory for SFE fluctuation; (ii) the energy fluctuation theory [21] adjusted for SFE; (iii) the definition of the physically relevant volume to SFE fluctuation; (iv) the Varvenne model [33] and (v) Peierls-Nabarro model [54]. The strengthening effect can be calculated following these equations without much computational effort. The full model is complicated to apply due to the coupling of these equations. For example, the number of atoms N_s determines the distribution of SFE; while SFE (its average) is also determined by N_s, leading to non-linear dependencies. These equations need to be solved self-consistently. As a reasonable approximation, we can consider N_s as a constant that is determined by the SFE at the experimental temperature γ_0. This removes some of the couplings. For NiCoCr and some other MPEAs, γ_0 =20–30 mJ mm^{-2} [20,41,42]. A value of 25mJ m^{-2} can be adopted to estimate the order of magnitude for strengthening through SFE fluctuation.

One of the key quantities to be firstly determined is $N_s = 2N_{(111)} \times \frac{\xi_c}{\sqrt{3}b} \times \frac{d_{12}}{b}$, with $N_{(111)} = 2$. The critical length $\xi_c = 20 - 35(\times\sqrt{3}b)$ (see Fig. 5(b) for NiCoCr and supplementary material for VCoNi and CoCrFeNiMn). For a general discussion, we take

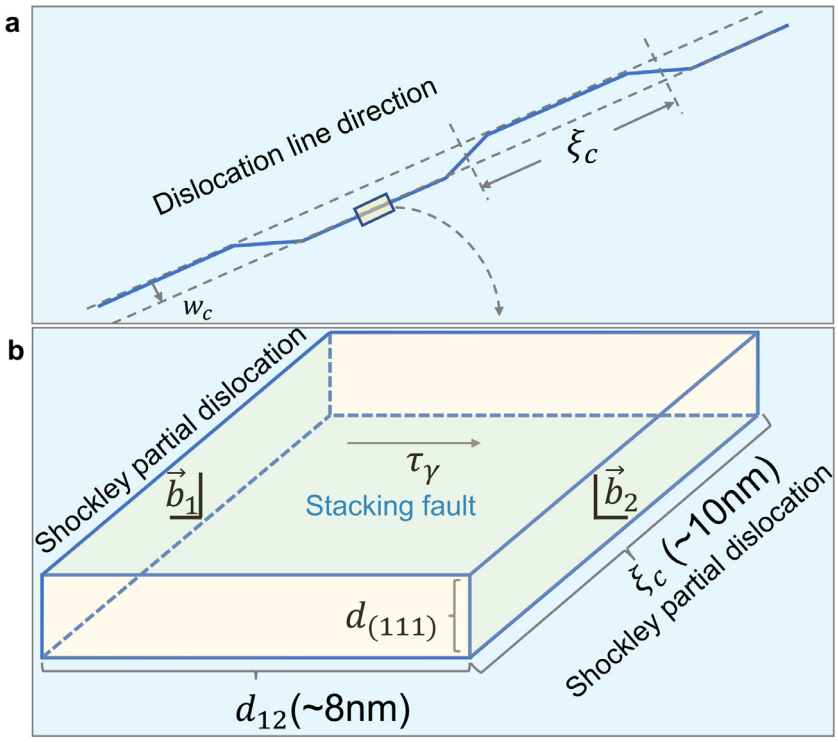

Fig. 4. Definition of the relevant region for the SFE fluctuation. (a) The geometric configuration of a typical dislocation in MPEAs, characterized by its critical glide distance on the slip plane w_c and critical segment of the length ξ_c that moves as a unit. (b) The supercell geometry for a dislocation segment. The energy fluctuation within the supercell is relevant to the stacking fault strengthening. $d_{(111)}$ is the distance between neighboring (111) planes, and d_{12} is the SF width. For the three MPEAs considered here, the larger two dimensions are about 8 nm and 10 nm.

Table 2
The strengthening effect through the SFE fluctuation at the nanoscale. The feature length is of the order of 10nm. The SFE standard variance by DFT are calculated with 30 configurations and in mJ m^{-2}.

parameter	NiCoCr	VCoNi	Cantor
γ (mJ m^{-2}) (298 K)	22 [42]	~30 [55]	30 [20]
Critical length, ξ_c (nm)	12.6	11.5	13.6
σ_{DFT} (mJ m^{-2})	72	86	88
σ_γ (mJ m^{-2})	5.0	8.1	7.1
$\sigma_{\Delta\gamma}$ (mJ m^{-2})	7.1	11.4	10.0
$\overline{\Delta\gamma}$ (mJ m^{-2})	5.7	9.1	8.0
b (Å)	2.51	2.56	2.54
$\tau_\gamma(C_0 = 1/\sqrt{\pi})$ (MPa)	22.6	35.7	31.5
$\tau_\gamma(C_0 = 1)$ (MPa)	40.0	63.3	55.7
$M\tau_\gamma(C_0 = 1/\sqrt{\pi})$ (MPa)	69	109	96
$M\tau_\gamma(C_0 = 1)$ (MPa)	122	194	171
CSRO effect (theory) (MPa) [a]	53	85	75
CSRO effect (experiment) (MPa) [10]	~50	-	-

[a] The CSRO effect is calculated by the difference $M\tau_\gamma(C_0 = 1) - M\tau_\gamma(C_0 = 1/\sqrt{\pi})$.

$\xi_c = 25\sqrt{3}b$. The SF width is estimated to be $d_{12} = 4 - 40b$, and a representative value is $20b$. Therefore, $N_s \approx 2000$.

For a typical ternary equiatomic alloy, $f(\{c_i\}) = \sum_i c_i \ln(c_i)$=1.099 and usually $\Delta E \in [0, 100]$ meV. For our general discussion we take $\Delta E = 50$ meV. If we know ΔE for a system, there is no need to perform DFT calculations to determine σ_γ. We can choose to use $\sigma_\gamma = \frac{\Delta E}{A\sqrt{2N_s f(\{c_i\})}}$, $A = 20b \times 25\sqrt{3}b = 500\sqrt{3}b^2$, $N_s = 2000$, so, $\sigma_\gamma = 14$mJ m^{-2}. For these values, we find $\tau_\gamma(C_0 = 1) = 53$ MPa, or $\tau_\gamma(C_0 = 1/\sqrt{\pi}) = 30$ MPa. However, since we usually do not know ΔE, DFT calculations are needed. Adopting DFT ($N_{\mathrm{DFT}} = 24$, details are presented in the supplementary material) to calculate $\sigma_{\gamma 1}$, we obtain 70–90 mJ m^{-2} (see Table 2). So, $\sigma_\gamma = 75\sqrt{24/2000} = 8.2$ mJ m^{-2}. $\tau_\gamma(C_0 = 1) = 2 \times 8.2/2.5 =$ 65 MPa or $\tau_\gamma(C_0 = 1/\sqrt{\pi}) = 2 \times 8.2/2.5 \times 1/\sqrt{\pi} = 37$ MPa. Considering the Taylor factor $M = 3.06$, we can find its contribution to the yield stresses is around 100 MPa.

3.4. Strengthening through the nanoscale SFE fluctuation in MPEAs

Assisted by the reduced model, the strengthening effects for the three representative MPEAs are calculated at room temperature (298K). The supercell size adopted in our DFT calculation is 72 atoms. For each alloy, 30 configurations are calculated to fully consider the randomness in a finite supercell, and guarantee that the standard variance σ_γ is converged [see supplementary material]. The number of atoms in the SF area is 12. Therefore $N_{\mathrm{DFT}} = 2 \times 12$=24. Following the equations in our model, the strengthening effect can be quantitatively determined.

The results are shown in Table 2. The strengthening effect through the SFE fluctuation is the most significant for VCoNi, which is 194 MPa, followed by the Cantor alloy with 171 MPa. These two alloys have comparable SFEs and σ_{DFT}, but VCoNi has a much lower shear modulus G resulting in a smaller SF width, smaller N_s and larger σ_γ and $\overline{\Delta\gamma}$. The solute solution strengthening effects for several alloys were calculated by Varvenne et al. [33] Compared to the solute solute strengthening effect without SFE fluctuations, the SFE strengthening is not small but comparable to the former.

4. Discussion

When SFE is positive and near zero, our model predicts a weak strengthening effect through SFE fluctuation. Similarly, when SFE becomes larger, this strengthening effect becomes more significant. This predicted trend is consistent with that by the model of Varvenne et al. [33] Note that the above conclusions are based on the

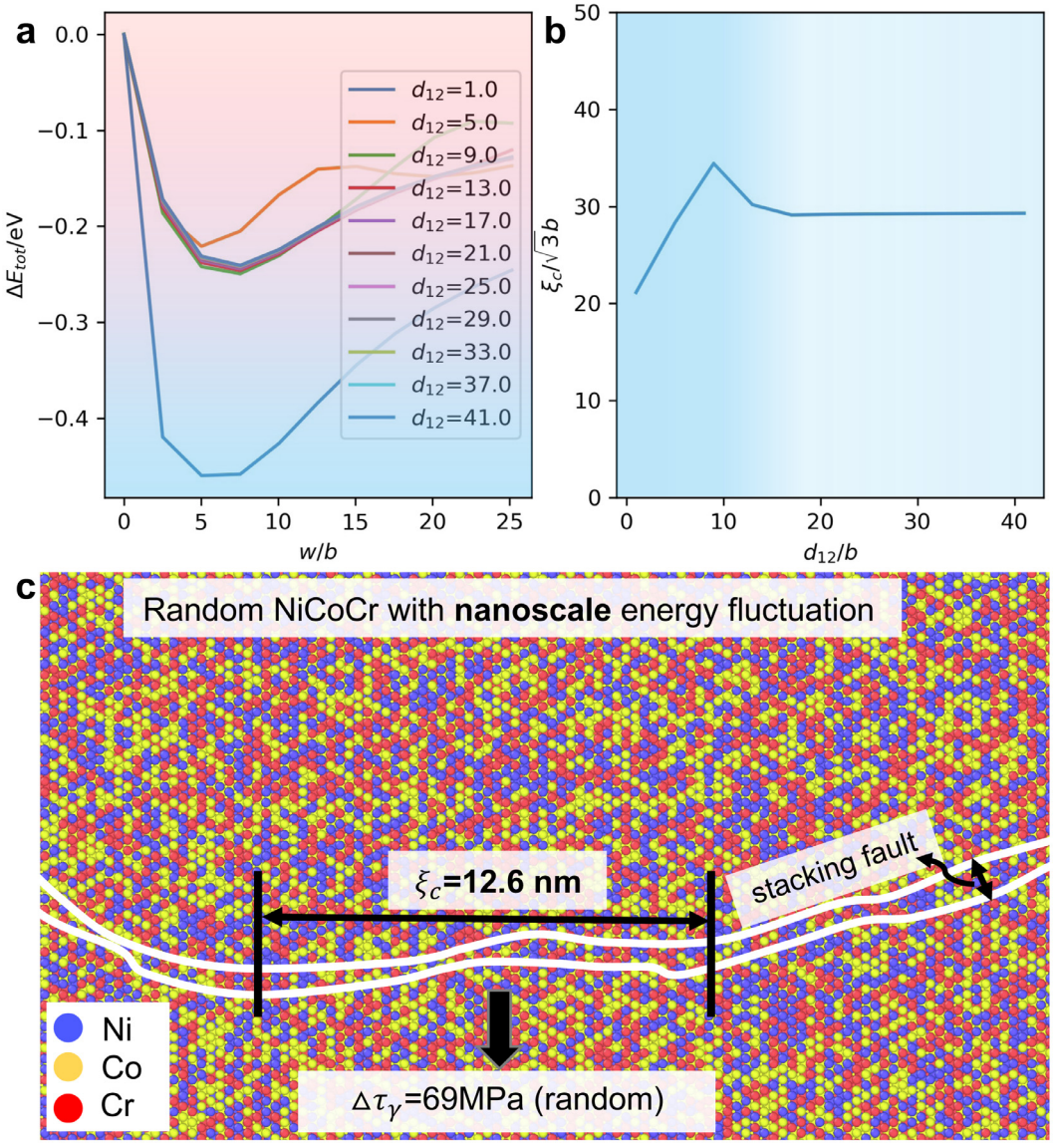

Fig. 5. The strengthening effect through the SFE fluctuation at the nanoscale. Here we take NiCoCr as an example. (a) Minimizing the total energy ΔE_{tot} to find the critical glide width w_c and critical length $\xi_c(w_c)$, for each d_{12}. (b) The critical length $\xi_c(w_c)$ as a function of SF width d_{12}. The critical length converges to a stable value of 12.6 nm ($29\sqrt{3}b$) at large d_{12}. The experimental half width of 1.23b is adopted for its Shockley partial dislocation [53]. (c) A schematic illustration for the strengthening through SFE fluctuation. The random state of NiCoCr is illustrated. The key ingredients to calculate the strengthening effect are also demonstrated.

classic configuration of Shockley partial dislocations (Fig. 1(b)), i.e., Case O in Ref. [16]. The case for a negative SFE is more complicated. When the two partials have a configuration as in Case O, their distance is theoretically infinite but experimentally finite in a non-equilibrium state. It can also be similar to that of the low SFEs when the two partials have a configuration of Case C, i.e., the two partials switch their positions. According to the mechanism of Case C [16], the strengthening effect can still be significant. In our method, the grain-size effect is not considered. Instead, we assume grains have sizes larger than the characteristic length of our model, which is of the order of 10nm. When grain sizes are smaller than the dimension of the relevant volume in Fig. 4, the smaller numbers need to be adopted.

The SFE distribution $N(\gamma)$ is also a function of the temperature. At low temperatures, CSRO may be present. The bonding preference of different chemical species promotes the SFE fluctuation and CSRO. However, no matter whether CSRO appears in a solid solution or not, the SFE fluctuation always contributes to solid-solution strengthening (Eq. (5)). CSRO in MPEAs has received substantial attention recently [10,12]. Fortunately, when CSRO exists, the SFE still follows the Gaussian distribution [44]. Hence, its effect can also be studied straightforwardly by the new model, assisted by affordable DFT calculations. The work of Zhang et al. shows a CSRO effect of about 50 MPa in the yield stress [10], which is comparable to our prediction of 53 MPa. It is worth mentioning that what our model predicts is one critical part of the total CSRO effects on the yield stress. CSRO can also affect the yielding of alloys through other contributions, such as lattice friction, solid-solution strengthening, and collaborative dislocation behaviors [10,56,57]. In addition, the important contribution to yield stress from lattice distortion has been addressed by other models [33,58], which are not discussed here. Since the model is based on the fluctuation of the stacking fault energy, when the full dislocation is dominant, the model is not applicable.

One unique feature of the new analytical model developed here is that it has no adjustable parameters. The model parameters can be determined either theoretically or experimentally. This model explains available experimental observations and provides insight-

ful guidance for the design of new MPEAs. Therefore it represents a significant advance in this direction.

5. Conclusions

MPEAs have received extensive attention due to their excellent mechanical properties. An essential feature of MPEAs is their chemical randomness associated with CSRO at the nanoscale. The CSRO and its impact on the mechanical properties of MPEAs have also received extensive attention. Its strengthening effect can be evaluated through the nanoscale SFE fluctuation within ∼10nm along the dislocation line. However, existing theories for conventional alloys cannot be used to quantify this strengthening effect in MPEAs, since such models [e.g., the Hirsch and Kelly model] require the unknown extreme values of SFE. We have developed an analytic model to quantify the strengthening effect in solid solutions due to this energy fluctuation. The model without adjustable parameters is generally applicable to solid solutions with various degrees of order, from random to short-range ordering states. It provides a pathway to tune the yield stress by increasing SFE fluctuations. It shows chemically very different atoms (such as these in VCoNi) offer a more significant fluctuation than similar ones (NiCoCr). Also, more principal elements tend to promote fluctuations. Our theory also shows that non-equiatomic systems have smaller configurational entropy and stronger fluctuations. These conclusions drawn from our model provide helpful guidance for the design of MPEAs through CSRO and, essentially, SFE fluctuations.

Data availability

All data are available in this paper or upon reasonable requests.

Declaration of Competing Interest

The authors declare that they have no known competing financial interests or personal relationships that could have appeared to influence the work reported in this paper.

Acknowledgements

The present work was sponsored by the U.S. Department of Energy, Office of Science, Basic Energy Sciences, Materials Science and Engineering Division. This research used resources of the Oak Ridge Leadership Computing Facility, which is supported by the Office of Science of the U.S. Department of Energy under Contract No. DE-AC05-00OR22725. P.K.L. very much appreciates the supports from (1) the National Science Foundation (DMR-1611180 and 1809640) with program directors, Drs. J. Yang, G. Shiflet, and D. Farkas and (2) the US Army Research Office (W911NF-13-1-0438 and W911NF-19-2-0049) with program managers, Drs. M.P. Bakas, S.N. Mathaudhu, and D.M. Stepp. M.C. acknowledges the support of U.S. National Science Foundation under grant DMR-1804320.

Supplementary material

Supplementary material associated with this article can be found, in the online version, at doi:10.1016/j.jmst.2023.01.042.

References

[1] X. Liu, J. Zhang, Z. Pei, Prog. Mater. Sci. 131 (2022) 101018.
[2] E.P. George, D. Raabe, R.O. Ritchie, Nat. Rev. Mater. 4 (8) (2019) 515–534.
[3] J.-W. Yeh, S.-K. Chen, S.-J. Lin, J.-Y. Gan, T.-S. Chin, T.-T. Shun, C.-H. Tsau, S.-Y. Chang, Adv. Eng. Mater. 6 (5) (2004) 299–303.
[4] B. Cantor, I. Chang, P. Knight, A. Vincent, Mater. Sci. Eng. A 375–377 (2004) 213–218.
[5] Y. Zhang, T.T. Zuo, Z. Tang, M.C. Gao, K.A. Dahmen, P.K. Liaw, Z.P. Lu, Prog. Mater. Sci. 61 (2014) 1–93.
[6] M.C. Gao, J.-W. Yeh, P.K. Liaw, Y. Zhang, High-Entropy Alloys, Springer International Publishing, 2016.
[7] E.P. George, W. Curtin, C.C. Tasan, Acta Mater. 188 (2020) 435–474.
[8] Q.-J. Li, H. Sheng, E. Ma, Nat. Commun. 10 (1) (2019) 1–11.
[9] X. Liu, Z. Pei, M. Eisenbach, Mater. Des. 180 (2019) 107955.
[10] R. Zhang, S. Zhao, J. Ding, Y. Chong, T. Jia, C. Ophus, M. Asta, R.O. Ritchie, A.M. Minor, Nature 581 (7808) (2020) 283–287.
[11] Q. Ding, Y. Zhang, X. Chen, X. Fu, D. Chen, S. Chen, L. Gu, F. Wei, H. Bei, Y. Gao, M. Wen, J. Li, Z. Zhang, T. Zhu, R.O. Ritchie, Q. Yu, Nature 574 (7777) (2019) 223–227.
[12] X. Chen, Q. Wang, Z. Cheng, M. Zhu, H. Zhou, P. Jiang, L. Zhou, Q. Xue, F. Yuan, J. Zhu, X. Wu, E. Ma, Nature 592 (7856) (2021) 712–716.
[13] H. Suzuki, J. Phys. Soc. Jpn. 17 (2) (1962) 322–325.
[14] G. Gottstein, Physical Foundations of Materials Science, Springer Science & Business Media, 2013.
[15] J.A. Yasi, L.G. Hector Jr, D.R. Trinkle, Acta Mater. 58 (17) (2010) 5704–5713.
[16] Z. Pei, B. Dutta, F. Körmann, M. Chen, Phys. Rev. Lett. 126 (25) (2021) 255502.
[17] Y. Zeng, X. Cai, M. Koslowski, Acta Mater. 164 (2019) 1–11.
[18] L. Zhang, Y. Xiang, J. Han, D.J. Srolovitz, Acta Mater. 166 (2019) 424–434.
[19] B. Yin, S. Yoshida, N. Tsuji, W. Curtin, Nat. Commun. 11 (1) (2020) 1–7.
[20] N.L. Okamoto, S. Fujimoto, Y. Kambara, M. Kawamura, Z.M. Chen, H. Matsunoshita, K. Tanaka, H. Inui, E.P. George, Sci. Rep. 6 (2016) 35863.
[21] Z. Pei, Scr. Mater. 162 (2019) 503–506.
[22] Q. Ding, Y. Zhang, X. Chen, X. Fu, D. Chen, S. Chen, L. Gu, F. Wei, H. Bei, Y. Gao, M. Wen, J. Li, Z. Zhang, T. Zhu, R.O. Ritchie, Q. Yu, Nature 574 (7777) (2019) 223–227.
[23] Y. Wu, F. Zhang, X. Yuan, H. Huang, X. Wen, Y. Wang, M. Zhang, H. Wu, X. Liu, H. Wang, S. Jiang, Z. Lu, J. Mater. Sci. Technol. 62 (2021) 214–220.
[24] M. Shih, J. Miao, M. Mills, M. Ghazisaeidi, Nat. Commun. 12 (1) (2021) 1–10.
[25] S. Chen, Z.H. Aitken, S. Pattamatta, Z. Wu, Z.G. Yu, D.J. Srolovitz, P.K. Liaw, Y.-W. Zhang, Nat. Commun. 12 (1) (2021) 1–11.
[26] S. Yin, Y. Zuo, A. Abu-Odeh, H. Zheng, X.-G. Li, J. Ding, S.P. Ong, M. Asta, R.O. Ritchie, Nat. Commun. 12 (1) (2021) 1–14.
[27] S. Chen, Z.H. Aitken, S. Pattamatta, Z. Wu, Z.G. Yu, R. Banerjee, D.J. Srolovitz, P.K. Liaw, Y.-W. Zhang, Acta Mater. 206 (2021) 116638.
[28] E. Antillon, C. Woodward, S. Rao, B. Akdim, T. Parthasarathy, Acta Mater. 190 (2020) 29–42.
[29] S.D. Wang, X.J. Liu, Z.F. Lei, D.Y. Lin, F.G. Bian, C.M. Yang, M.Y. Jiao, Q. Du, H. Wang, Y. Wu, S.H. Jiang, Z.P. Lu, Phys. Rev. B 103 (2021) 104107.
[30] X. Liu, H. Zhao, H. Ding, D.-Y. Lin, F. Tian, Appl. Phys. Lett. 119 (13) (2021) 131904.
[31] P.B. Hirsch, A. Kelly, Philos. Magaz. A 12 (119) (1965) 881–900.
[32] E. Nembach, Scr. Metall. 20 (5) (1986) 763–768.
[33] C. Varvenne, A. Luque, W.A. Curtin, Acta Mater. 118 (2016) 164–176.
[34] P. Hohenberg, W. Kohn, Phys. Rev. 136 (1964) B864.
[35] W. Kohn, L.J. Sham, Phys. Rev. 140 (1965) A1133.
[36] G. Kresse, J. Furthmüller, Phys. Rev. B 54 (1996) 11169–11186.
[37] J.P. Perdew, K. Burke, M. Ernzerhof, Phys. Rev. Lett. 77 (1996) 3865–3868.
[38] P.E. Blöchl, Phys. Rev. B 50 (1994) 17953–17979.
[39] H.J. Monkhorst, J.D. Pack, Phys. Rev. B 13 (1976) 5188–5192.
[40] S.S. Sohn, A. Kwiatkowski da Silva, Y. Ikeda, F. Körmann, W. Lu, W.S. Choi, B. Gault, D. Ponge, J. Neugebauer, D. Raabe, Adv. Mater. 31 (8) (2019) 1807142.
[41] A. Zaddach, C. Niu, C. Koch, D. Irving, JOM 65 (12) (2013) 1780–1789.
[42] G. Laplanche, A. Kostka, C. Reinhart, J. Hunfeld, G. Eggeler, E. George, Acta Mater 128 (2017) 292–303.
[43] S. Rao, B. Akdim, E. Antillon, C. Woodward, T. Parthasarathy, O. Senkov, Acta Mater. 168 (2019) 222–236.
[44] J. Ding, Q. Yu, M. Asta, R.O. Ritchie, Proc. Natl. Acad. Sci. 115 (36) (2018) 8919–8924.
[45] Z. Pei, M. Eisenbach, S. Mu, G.M. Stocks, Comput. Phys. Commun. 235 (2019) 95–101.
[46] S.N. Khan, M. Eisenbach, Phys. Rev. B 93 (2016) 024203.
[47] S. Zhao, Y. Osetsky, G.M. Stocks, Y. Zhang, npj Comput. Mater. 5 (1) (2019) 1–7.
[48] A. Zunger, S.-H. Wei, L.G. Ferreira, J.E. Bernard, Phys. Rev. Lett. 65 (3) (1990) 353.
[49] D. Ma, M. Friák, J. von Pezold, J. Neugebauer, D. Raabe, Acta Mater. 98 (2015) 367–376.
[50] G.P.M. Leyson, W.A. Curtin, L.G. Hector, C.F. Woodward, Nat. Mater. 9 (9) (2010) 750–755.
[51] A. Tehranchi, B. Yin, W. Curtin, Acta Mater. 151 (2018) 56–66.
[52] C. Varvenne, G.P.M. Leyson, M. Ghazisaeidi, W.A. Curtin, Acta Mater 124 (2017) 660–683.
[53] Z. Pei, S. Zhang, Y. Lei, F. Zhang, M. Chen, Proc. Natl. Acad. Sci. 118 (51) (2021) e2114167118.
[54] P.M. Anderson, J.P. Hirth, J. Lothe, Theory of Dislocations, Cambridge University Press, 2017.
[55] D.C. Yang, Y.H. Jo, Y. Ikeda, F. Körmann, S.S. Sohn, J. Mater. Sci. Technol. 90 (2021) 159–167.
[56] V. Gerold, H. Karnthaler, Acta Metall. 37 (8) (1989) 2177–2183.
[57] T. Neeraj, M. Mills, Mater. Sci. Eng. A 319 (2001) 415–419.
[58] I. Toda-Caraballo, P.E.R.-D. del Castillo, Acta Mater. 85 (2015) 14–23.